JOURNAL OF THERMOPHYSICS AND HEAT TRANSFER
Vol. 17, No. 4, October–December 2003

Modified One-Equation Turbulence Models for Turbulent Magnetohydrodynamic Flows

Jean-François Dietiker* and Klaus A. Hoffmann†
Wichita State University, Wichita, Kansas 67260-0044

The Baldwin–Barth and Spalart–Allmaras one-equation turbulence models are implemented to solve turbulent magnetohydrodynamic (MHD) flows. Because the original version of these turbulence models were not designed for MHD flows, some modifications are proposed to include the effect of the magnetic field on turbulence. In the case of the Baldwin–Barth model, an additional magnetic term is introduced into the turbulence model equation, whereas one of the closure coefficients is made dependent on the magnetic field for the Spalart–Allmaras model. The MHD equations are considered under the low magnetic Reynolds number approximation, that is, for low electrical conductivity fluids. The proposed modifications associated with the magnetic field are calibrated based on the turbulent Hartmann flow. The modified versions are able to predict accurately the experimentally observed relaminarization process at *Ha*/*Re* = 1/225. Investigation of the supersonic flow over a flat plate shows that a substantial reduction in the skin friction can be achieved; however, no relaminarization process was observed for the range of applied magnetic fields.

Nomenclature

B = magnitude of the magnetic induction field
$\boldsymbol{B}$ = magnetic induction field,

$$\begin{bmatrix} B_x \\ B_y \\ B_z \end{bmatrix}$$

C'_{kN1} = closure coefficient in modified $k-\epsilon$ turbulence model
C_{Re_T} = closure coefficient in modified Baldwin–Barth model
$C'_{\epsilon N1}$ = closure coefficient in modified $k-\epsilon$ model
c_p = specific heat at constant pressure
D_1, D_2 = damping functions
d = distance to the nearest wall
e_t = total energy per unit mass
$\boldsymbol{E}$ = flux vector in x direction (physical space)
$\boldsymbol{E}_c$ = electric field vector,

$$\begin{bmatrix} E_x \\ E_y \\ E_z \end{bmatrix}$$

$\boldsymbol{E}_v$ = viscous flux vector in x direction (physical space)
$\bar{\boldsymbol{E}}$ = flux vector in ξ direction (computational space)
$\bar{\boldsymbol{E}}_v$ = viscous flux vector in ξ direction (computational space)
$\boldsymbol{F}$ = flux vector in y direction (physical space)
$\boldsymbol{F}_v$ = viscous flux vector in y direction (physical space)
$\bar{\boldsymbol{F}}$ = flux vector in η direction (computational space)
$\bar{\boldsymbol{F}}_v$ = viscous flux vector in η direction (computational space)
Ha = Hartmann number
J = Jacobian of transformation
$\boldsymbol{J}$ = current density vector
k = thermal conductivity, turbulent kinetic energy
L = characteristic length
M_k = additional magnetic term in the k equation
M_ϵ = additional magnetic term in the ϵ equation
M_∞ = freestream Mach number
m = interaction number per unit length
N = interaction parameter
P_k = production term
Pr = prandtl number
p = pressure
$\boldsymbol{Q}$ = vector of conserved variables
$\boldsymbol{Q}_h$ = heat flux vector

$$\begin{bmatrix} q_x \\ q_y \\ q_z \end{bmatrix}$$

$\bar{\boldsymbol{Q}}$ = vector of conserved variables in computational space
Re = Reynolds number
Re_m = magnetic Reynolds number
Re_T = turbulent Reynolds number
S = absolute value of vorticity
$\boldsymbol{S}_{\mathrm{MHD}}$ = MHD source term in physical space
$\bar{\boldsymbol{S}}_{\mathrm{MHD}}$ = MHD source term in computational space
T = temperature
t = time
U = magnitude of the velocity vector
$\boldsymbol{U}$ = velocity vector

$$\begin{bmatrix} u \\ v \\ w \end{bmatrix}$$

x, y = space coordinates
y^+ = nondimensional distance to the wall
γ = ratio of specific heats
δ_{ij} = Kronecker delta
ϵ = dissipation rate of turbulent kinetic energy
η_x, η_y = metrics of transformation
μ = dynamic viscosity
μ_{e0} = free space magnetic permeability
μ_t = turbulent dynamic viscosity

Received 5 February 2003; revision received 28 April 2003; accepted for publication 28 April 2003.

*Visiting Assistant Professor, Department of Aerospace Engineering, 1845 Fairmount. Member AIAA.
†Professor, Department of Aerospace Engineering, 1845 Fairmount. Associate Fellow AIAA.

ν = kinematic viscosity
ν_e = magnetic diffusivity
ν_t = turbulent kinematic viscosity
$\bar{\nu}$ = turbulent variable in Spalart–Allmaras model
ξ, η = generalized coordinates (computational space)
ξ_x, ξ_y = metrics of transformation
ρ = density
σ_e = electrical conductivity
$\bar{\bar{\tau}}$ = stress tensor

Subscripts

w = property evaluated at the wall
∞ = freestream condition

Superscripts

$'$ = perturbation quantity
$*$ = nondimensional quantity
$-$ = Reynolds averaged quantity, quantity expressed in computational space

I. Introduction

MAGNETOHYDRODYNAMICS (MHD) is the study of an electrically conducting fluid subject to an electromagnetic field. The interaction between the magnetic field and velocity field generates an induced electric field and, subsequently, an electric current. The combination of the induced electric current and the electromagnetic field creates a body force, called the Lorentz force (or ponderomotive force). This body force acts on the fluid, which offers a new mean of flow control. From an engineering prospect, magnetohydrodynamics can be beneficially utilized in a wide variety of applications, ranging from propulsion systems to power generators. It also shows great potential in aerospace applications by offering the possibility of controlling the flow around a vehicle or even extracting energy from its surrounding.

MHD has been the subject of numerous investigations. In the early stages toward the understanding of the MHD effect, analytical or empirical methods were developed to solve the governing equations. However, because of the nature of the equations, they could be solved only for simple flows with restrictive assumptions on the flow or the magnetic field. The solution for an incompressible laminar flow over a flat plate, subject to a uniform magnetic field, was solved by Rossow.[1] He showed that the skin friction and heat transfer are reduced when the magnetic field is increased. The same trend has been observed by other investigators. Lykoudis developed a similarity solution for boundary-layer flows over a wedge.[2] The hypersonic MHD couette flow was analytically solved by Bleviss.[3] He found that, for high Mach numbers, the presence of a magnetic field decreases the skin friction but increases the heat transfer. Bush studied hypersonic flows around blunt bodies[4] and showed that the shock standoff distance would increase and the surface pressure would decrease in the presence of a magnetic field. Lykoudis[5] developed an analytical solution for the shock standoff distance for hypersonic flows of an electrically conducting fluid around a sphere and a cylinder.

With the emergence of numerical tools such as computational fluid dynamics, MHD flows can be investigated under less limiting conditions on the magnetic field or the flow properties. Palmer[6] numerically solved the flow past an axisymmetric blunt body and verified the increase in the standoff distance as predicted by analytical solutions. Because of the hyperbolic nature of MHD equations, numerical schemes based on characteristic formulation have been widely used. High-order Godunov schemes have been used for one-dimensional and shock tube problems (see Refs. 7–12). More recently, modified Runge–Kutta schemes augmented with total variation diminishing (TVD) schemes have been used for one-dimensional and two-dimensional problems (see Refs. 13–17). TVD schemes allow good shock wave capturing with little or no spurious oscillations. This method requires the determination of the eigenvalues and eigenvectors of the system of equations. For the ideal one-dimensional case, it results in a seven-wave system, whereas for the ideal two-dimensional case, an eight-wave system is obtained. It has been shown that the determination of the eigenvalues and eigenvectors of the system requires a mathematical modification of the governing equations due to a singularity in the Jacobian matrices (see Ref. 18). Recently, this scheme has been extended to the case where molecular viscosity and magnetic diffusivity are taken into consideration.[19]

The inclusion of turbulence in the computation of MHD flowfields is a natural step toward a better understanding of MHD. It is widely accepted that the presence of a magnetic field could decrease the drag and heat transfer for laminar flows. On the other hand, turbulence is associated with an increase in drag and heat transfer. Thus, it is important to investigate turbulent flowfields subject to magnetic fields to identify the overall effect of this combination.

Most of the research combining the effect of turbulence with MHD has been conducted for flows of liquid metals in simple geometries or in astrophysical applications, where the length scales are very large. Basic observations tend to show that the presence of a magnetic field would inhibit turbulence.[20,21]

For simple engineering applications, the effect of the magnetic field on turbulence has been integrated into existing turbulence concepts or even turbulence models. Lykoudis[22] generalized the Prandtl mixing length concept to MHD for a fully established turbulent channel flow, in a transverse and uniform magnetic field (electrically insulated channel). Damping functions are introduced into the expression for the turbulent stress to take the presence of a magnetic field into account. Several authors have used the $k-\epsilon$ two-equation model in conjunction with MHD flows.[23–26] Shimomura[27] derived the equations for the turbulent kinetic energy and its dissipation rate based on the two-scale direct interaction approximation approach. The resulting equations, although exact, are very complex and require several closure coefficients, which cannot be clearly determined. However, in some cases, simplifications based on the geometry of the problem can be made. The modified $k-\epsilon$ includes additional magnetic terms that represent the MHD effect on turbulence.

There are mainly three approaches for the computation of turbulent flows. The direct numerical simulation (DNS) approach is an "exact method" in the sense that the original governing equations are solved without any modifications, or filtering process. When it is assumed that the error introduced by the numerical scheme used to solve these equations can be evaluated or controlled, the use of DNS can provide high-quality results, equivalent to an experiment.

The second approach for turbulent flow computation is the large eddy simulation.[28] Large scales are numerically computed, whereas the small scales are modeled by eddy viscosity models, known as subgrid-scale models. Algebraic models are sufficient because the imperfections of these simple models should not greatly affect the solution.

The two methods just described are very costly in terms of computational time and storage requirement. A more affordable method consists in averaging the Navier–Stokes equations in time (also called Reynolds averaging). When the filter operation is applied to the equations, the Reynolds-averaged Navier–Stokes (RANS) equations are obtained. In this filtering process, additional terms appear, known as the Reynolds stresses. A closure model (or turbulence model) is required to close the system. A tremendous amount of investigation has been conducted in this domain, resulting in many different turbulence models, ranging from simple algebraic models to more sophisticated multi-equation models.[29] Unfortunately, none of the proposed models is able to predict accurately turbulent flows over a wide range of applications. The difficulty in developing such models lies in that the closure constants are based on empiricism and are calibrated to match the experimental data. This makes them nonuniversal and more likely to provide good results only for the type of applications they were designed for.

The RANS approach is used for simple engineering applications because of its relatively low computational cost compared to other existing methods. Because the turbulence models used in RANS

are mostly based on empiricism, they have to be tuned for a given application.

The objective of this investigation is to propose modifications to the Baldwin–Barth[30] and Spalart–Allmaras[31] one-equation turbulence models and extend their validity to MHD flows. The Baldwin–Barth model is derived from the modified $k-\epsilon$ model, in which additional magnetic terms represent the MHD effect on turbulence. The Spalart–Allmaras turbulence model is modified by enforcing the dependency of one of the closure coefficient on the magnetic field. The modified turbulence models are calibrated from the turbulent Hartmann flow, for which experimental evidence of a relaminarization process has been observed. The supersonic flow over a flat plate is numerically simulated to investigate the effect of the magnetic field on the skin-friction coefficient distribution.

II. Governing Equations

The MHD equations are obtained by combining Maxwell's equations, Ohm's law, and the Navier–Stokes equations. Maxwell's equations relate the basic electric and magnetic field quantities and how they are produced. The Navier–Stokes equations describe the motion of the fluid. The combination of Maxwell's equations and Ohm's law results in what is referred to as the magnetic transport equation. The resulting system of equations, therefore, comprises eight equations: continuity, momentum (three components), energy, and magnetic field induction (three components). However, for low electrical conductivity fluids, the governing equations can be simplified, provided that the magnetic Reynolds number is small compared to one. The magnetic Reynolds number is defined as $Re_{m\infty}=\sigma_{e\infty}\mu_{e0}U_\infty L$, where $\sigma_{e\infty}$ is the electrical conductivity of the fluid, μ_{e0} is the magnetic permeability, and U_∞ and L are the reference velocity and length scale, respectively. The magnetic Reynolds number represents the ratio of the magnetic convection to the magnetic diffusion. For small values ($Re_{m\infty}<<1$), it can be shown that the induced magnetic field is negligible compared to the applied magnetic field. Therefore, when this assumption is valid, the magnetic induction equations do not need to be solved, and the number of equations is reduced to five. This is especially appealing because the method applied to solve the magnetic induction equations is the source of numerical difficulties. When the full system of MHD equations is solved, it has been experienced to be very difficult for the magnetic field solution to remain divergence free at all time levels. Numerical techniques have been proposed to alleviate this problem,[18] but generally result in more complex equations or additional steps in the numerical procedure. In the low magnetic Reynolds number approach, the magnetic field is a given quantity and automatically satisfies the zero-divergence constraint. The current density is determined from Ohm's law, and the MHD effect is modeled by the introduction of source terms in the Navier–Stokes equations. The MHD equations are nondimensionalized for ease of numerical solution using the following variables:

$$(x^*, y^*)=\frac{(x, y)}{L},\qquad t^*=\frac{U_\infty t}{L},\qquad (u^*, v^*, w^*)=\frac{(u, v, w)}{U_\infty}$$

$$\rho^*=\frac{\rho}{\rho_\infty},\qquad p^*=\frac{p}{\rho_\infty U_\infty^2},\qquad \left(B_x^*, B_y^*, B_z^*\right)=\frac{(B_x, B_y, B_z)}{U_\infty\sqrt{\mu_{e0}\rho_\infty}}$$

$$T^*=\frac{T}{T_\infty},\qquad e_t^*=\frac{e_t}{U_\infty^2},\qquad \bar{\bar{\tau}}^*=\frac{\bar{\bar{\tau}}L}{\mu_\infty U_\infty}$$

$$\mu_{e0}^*=\frac{\mu_{e0}}{\mu_{e0}}=1,\qquad \sigma_e^*=\frac{\sigma_e}{\sigma_{e\infty}},\qquad \nu_e^*=\frac{\nu_e}{\nu_{e\infty}},\qquad \mu^*=\frac{\mu}{\mu_\infty}$$

In the following sections, the asterisk superscript designating nondimensional quantities will be dropped for convenience. Therefore, all of the equations will be written in nondimensional form, unless specifically stated.

Under the assumption of small magnetic Reynolds number, the governing equations are as follows.

Continuity:

$$\frac{\partial\rho}{\partial t}+\nabla\cdot(\rho\boldsymbol{U})=0 \tag{1}$$

Momentum:

$$\frac{\partial(\rho\boldsymbol{U})}{\partial t}+\nabla\cdot[\rho\boldsymbol{U}\otimes\boldsymbol{U}+p\bar{\bar{\boldsymbol{I}}}]=\frac{1}{Re_\infty}\nabla\cdot\bar{\bar{\boldsymbol{\tau}}}+Re_{m_\infty}\boldsymbol{J}\times\boldsymbol{B} \tag{2}$$

Energy:

$$\frac{\partial}{\partial t}(\rho e_t)+\nabla\cdot[(\rho e_t+p)\boldsymbol{U}]=\frac{1}{Re_\infty}\nabla\cdot(\boldsymbol{U}\cdot\bar{\bar{\boldsymbol{\tau}}})$$
$$-\frac{1}{(\gamma-1)PrM^2Re_\infty}\nabla\cdot\boldsymbol{Q}_h+Re_{m_\infty}\boldsymbol{E}_c\cdot\boldsymbol{J} \tag{3}$$

The current density is evaluated from Ohm's law:

$$\boldsymbol{J}=\sigma_e(\boldsymbol{E}_c+\boldsymbol{U}\times\boldsymbol{B}) \tag{4}$$

For a Newtonian fluid,

$$\tau_{ij}=\frac{\mu}{Re_\infty}\left(\frac{\partial u_i}{\partial x_j}+\frac{\partial u_j}{\partial x_i}-\frac{2}{3}\frac{\partial u_k}{\partial x_k}\delta_{ij}\right) \tag{5}$$

and for a perfect gas

$$q_i=-\frac{\mu}{Re_\infty Pr(\gamma-1)M_\infty^2}\frac{\partial T}{\partial x_i} \tag{6}$$

The nondimensional parameters appearing in the equations are the Reynolds number $Re_\infty=\rho_\infty U_\infty L/\mu_\infty$, the Prandtl number $Pr=\mu_\infty c_p/k$, the magnetic Reynolds number $Re_{m\infty}=\sigma_{e\infty}\mu_{e0}U_\infty L$, and the freestream Mach number $M_\infty=U_\infty/\sqrt{(\gamma p_\infty/\rho_\infty)}$. The Hall effect and ion slip are neglected in the present investigation. (Typical values of the Hall parameter and ion slip parameter are between 1 and 5, in nondimensional form.)

A. Flux Vector Formulation

The equations are solved by using an extended two-dimensional approach. Although three spatial components of the velocity and magnetic and electric fields are considered for the evaluation of the magnetic source terms (the Lorentz force requires the computation of several cross products), all flow variables are assumed to vary in only two dimensions. Therefore, only two spatial derivatives are taken into account. The system of equations is written in a flux vector formulation as

$$\frac{\partial\boldsymbol{Q}}{\partial t}+\frac{\partial\boldsymbol{E}}{\partial x}+\frac{\partial\boldsymbol{F}}{\partial y}=\frac{\partial\boldsymbol{E}_v}{\partial x}+\frac{\partial\boldsymbol{F}_v}{\partial y}+\boldsymbol{S}_{\mathrm{MHD}} \tag{7}$$

where $\boldsymbol{Q}$ is the unknown vector, $\boldsymbol{E}$ and $\boldsymbol{F}$ are the inviscid flux vectors, and $\boldsymbol{E}_v$ and $\boldsymbol{F}_v$ are the viscous flux vectors. The additional source term is represented by $\boldsymbol{S}_{\mathrm{MHD}}$. The unknown and flux vectors are given by Eqs. (8a–8f). The unknown quantities that need to be computed are the density, momentum components, and total energy. The magnetic and electric fields are considered as given quantities and remain constant throughout the computations. Thus,

$$\boldsymbol{Q} = \begin{bmatrix} \rho & \rho u & \rho v & \rho w & \rho e_t \end{bmatrix}^T \tag{8a}$$

$$\boldsymbol{E} = \begin{bmatrix} \rho u \\ \rho u^2 + p \\ \rho uv \\ \rho uw \\ (\rho e_t + p)u \end{bmatrix}, \qquad \boldsymbol{F} = \begin{bmatrix} \rho v \\ \rho vu \\ \rho v^2 + p \\ \rho vw \\ (\rho e_t + p)v \end{bmatrix} \tag{8b}$$

$$\boldsymbol{E}_v = \begin{bmatrix} 0 \\ \tau_{xx} \\ \tau_{xy} \\ \tau_{xz} \\ u\tau_{xx} + v\tau_{xy} + w\tau_{xz} - q_x \end{bmatrix}, \qquad \boldsymbol{F}_v = \begin{bmatrix} 0 \\ \tau_{yx} \\ \tau_{yy} \\ \tau_{yz} \\ u\tau_{yx} + v\tau_{yy} + w\tau_{yz} - q_y \end{bmatrix} \tag{8c}$$

$$\boldsymbol{S}_{\mathrm{MHD}} = Re_{m_\infty} \begin{bmatrix} 0 \\ B_z(E_y + wB_x - uB_z) - B_y(E_z + uB_y - vB_x) \\ B_x(E_z + uB_y - vB_x) - B_z(E_x + vB_z - wB_y) \\ B_y(E_x + vB_z - wB_y) - B_x(E_y + wB_x - uB_z) \\ E_x(E_x + vB_z - wB_y) + E_y(E_y + wB_x - uB_z) + E_z(E_z + uB_y - vB_x) \end{bmatrix} \tag{8d}$$

where

$$\rho e_t = \tfrac{1}{2}\rho(u^2 + v^2 + w^2) + p/(\gamma - 1) \tag{9}$$

B. Generalized Coordinates

The governing MHD equation given by Eq. (7), which is written in the physical space (x, y), is transformed into the computational space (ξ, η) and expressed as

$$\frac{\partial \bar{\boldsymbol{Q}}}{\partial t} + \frac{\partial \bar{\boldsymbol{E}}}{\partial \xi} + \frac{\partial \bar{\boldsymbol{F}}}{\partial \eta} = \frac{\partial \bar{\boldsymbol{E}}_v}{\partial \xi} + \frac{\partial \bar{\boldsymbol{F}}_v}{\partial \eta} + \bar{\boldsymbol{S}}_{\mathrm{MHD}} \tag{10}$$

where

$$\bar{\boldsymbol{Q}} = \boldsymbol{Q}/J \tag{11a}$$

$$\bar{\boldsymbol{E}} = (1/J)(\xi_x \boldsymbol{E} + \xi_y \boldsymbol{F}), \qquad \bar{\boldsymbol{F}} = (1/J)(\eta_x \boldsymbol{E} + \eta_y \boldsymbol{F}) \tag{11b}$$

$$\bar{\boldsymbol{E}}_v = (1/J)(\xi_x \boldsymbol{E}_v + \xi_y \boldsymbol{F}_v), \qquad \bar{\boldsymbol{F}}_v = (1/J)(\eta_x \boldsymbol{E}_v + \eta_y \boldsymbol{F}_v) \tag{11c}$$

$$\bar{\boldsymbol{S}}_{\mathrm{MHD}} = (1/J)\boldsymbol{S}_{\mathrm{MHD}} \tag{11d}$$

where J is the Jacobian of transformation defined as

$$J = \frac{\partial(\xi, \eta)}{\partial(x, y)} \tag{11e}$$

III. Numerical Scheme

The governing equations are solved by a four-stage Runge–Kutta scheme. It has been selected because of its high order of temporal accuracy (fourth-order) and its low storage requirement because only two time levels need to be stored. The spatial derivatives are approximated by second-order central differences. Details about the numerical scheme may be found in Ref. 17.

Some instability may arise due to the high order of spatial accuracy associated with the numerical scheme. To alleviate this problem, a postprocess stage is usually required to stabilize the solution. A method that has been successfully employed in the past is the application of a TVD scheme as a postprocess stage. This method has the advantage of automatically adjusting the amount of damping (by switching from second to first order in accuracy) where needed. However, it requires the computation of the eigenvalues and eigenvectors associated with the governing equations. It is also expensive in terms of computational resources. The second-order symmetric TVD scheme with Davis–Yee symmetric limiter has been chosen due to its successful application to MHD problems by previous investigators (see Ref. 17). It is particularly appealing for high-speed problems involving strong discontinuities such as shock waves. Details of the postprocess stage may be found in Ref. 19.

When a steady-state solution is sought, it is possible to accelerate the convergence of the solution by specifying a local time step at each grid point. This allows the solution to march faster where the eigenvalues of the system are small, that is, the characteristic speeds of the wave propagation are small. The time step is locally computed as a function of the eigenvalues of the system, the computational grid spacing, and the Courant–Friedrichs–Lewy (CFL) number, which is a user-specified parameter. For stability purposes, the range of CFL number is typically specified between 0.05 and 0.2. The convergence criterion is based on the change in pressure between two successive iterations, calculated over the entire domain of solution. Convergence is achieved when the change in pressure has decreased by four orders of magnitude.

IV. Turbulence Models

A. Baldwin–Barth One-Equation Turbulence Model

The Baldwin–Barth turbulence model[30] is a one-equation model derived from the $k - \epsilon$ model. It requires the solution of a transport partial differential equation for a new variable that is the product of the kinematic viscosity and the turbulent Reynolds number defined as $Re_T = k^2/\nu\epsilon$. For flows in the near-wall region, the turbulent Reynolds number is split into $Re_T = \overline{Re_T} f(\overline{Re_T})$, where f is a damping function allowing Re_T and $\overline{Re_T}$ to be equal for large values of Re_T. The transport equation in terms of $\nu\overline{Re_T}$ is given by

$$\frac{\mathrm{D}}{\mathrm{D}t}(\nu\overline{Re_T}) = (C_{\epsilon 2} f_2 - C_{\epsilon 1})\sqrt{\nu\overline{Re_T} P_k} + \left(\nu + \frac{\nu_t}{\sigma_\epsilon}\right)\nabla^2(\nu\overline{Re_T}) - \frac{1}{\sigma_\epsilon}(\nabla\nu_t)\cdot\nabla(\nu\overline{Re_T}) \tag{12}$$

Once this equation is solved, the turbulent viscosity is determined from

$$\mu_t = \rho c_\mu (\nu\overline{Re_T}) D_1 D_2 \tag{13}$$

The two damping functions D_1 and D_2 are used to extend the model to the near-wall region. They are

$$D_1 = 1 - \exp(-y^+/A^+) \tag{14}$$

$$D_2 = 1 - \exp\left(-y^+ \big/ A_2^+\right) \tag{15}$$

The production term is given by

$$P_k = \nu_t\left(\frac{\partial u_i}{\partial x_j} + \frac{\partial u_j}{\partial x_i}\right)\frac{\partial u_i}{\partial x_j} - \frac{2}{3}\nu_t\left(\frac{\partial u_k}{\partial x_k}\right)^2 \tag{16}$$

The function f_2 is given by

$$f_2(y^+) = \frac{c_{\epsilon 1}}{c_{\epsilon 2}} + \left(1 - \frac{c_{\epsilon 1}}{c_{\epsilon 2}}\right)\left(\frac{1}{\kappa y^+} + D_1 D_2\right) \times \left\{\sqrt{D_1 D_2} + \frac{y^+}{\sqrt{D_1 D_2}}\left[\frac{D_2}{A^+}\exp\left(-\frac{y^+}{A^+}\right) + \frac{D_1}{A_2^+}\exp\left(-\frac{y^+}{A_2^+}\right)\right]\right\} \tag{17}$$

and the closure coefficients are as follows:

$$\kappa = 0.41, \qquad c_{\epsilon 1} = 1.2, \qquad c_{\epsilon 2} = 2.0, \qquad c_\mu = 0.09,$$

$$A^+ = 26, \qquad A_2^+ = 10, \qquad 1/\sigma_\epsilon = (c_{\epsilon 2} - c_{\epsilon 1})\sqrt{c_\mu}\big/\kappa^2$$

B. Spalart–Allmaras One-Equation Model

The Spalart–Allmaras turbulence model is a one-equation model that solves a partial differential equation for the variable $\bar{\nu}$, which is related to the turbulent viscosity. The model is based on "empiricism, dimensional analysis, and selective dependence on molecular viscosity."[31] The transport equation for the variable $\bar{\nu}$ is

$$\frac{\mathrm{D}\bar{\nu}}{\mathrm{D}t} = C_{b1}(1 - f_{t2})\bar{S}\bar{\nu} + \frac{1}{\sigma}\left\{\nabla[(\nu + \bar{\nu})\nabla\bar{\nu}] + C_{b2}(\nabla\bar{\nu})^2\right\} + \frac{C_{b1}}{\kappa^2}f_{t2}\left(\frac{\bar{\nu}}{d}\right)^2 - C_{w1}f_w\left(\frac{\bar{\nu}}{d}\right)^2 + f_{t1}(\Delta q)^2 \tag{18}$$

This equation states that the total change in turbulent viscosity is equal to the sum of production, dissipation, diffusion, and destruction of turbulent viscosity. The model also includes a trip function for transition from laminar to turbulent flow.

The kinematic turbulent viscosity is determined from

$$\nu_t = \bar{\nu} f_{v1} \tag{19}$$

where

$$f_{v1} = \chi^3\big/\left(\chi^3 + C_{v1}^3\right) \tag{20}$$

$$\chi = \bar{\nu}/\nu \tag{21}$$

$$\bar{S} = S + (\bar{\nu}/\kappa^2 d^2) f_{v2} \tag{22}$$

$$f_{v2} = 1 - \chi/(1 + \chi f_{v1}) \tag{23}$$

where d is the distance to the wall and S is the magnitude of the vorticity,

$$S = |\omega| = \left|\frac{\partial\bar{v}}{\partial x} - \frac{\partial\bar{u}}{\partial y}\right| \tag{24}$$

$$f_w = g\left(\frac{1 + C_{w3}^6}{g^6 + C_{w3}^6}\right)^{\frac{1}{6}} \tag{25}$$

where

$$g = r + C_{w2}(r^6 - r) \tag{26}$$

$$r = \bar{\nu}/\bar{S}\kappa^2 d^2 \tag{27}$$

A final set of terms includes control over the laminar regions and the transition. They maintain laminar flow where required and include transition at a specified location. In the laminar region, $\bar{\nu}$ must be of the order of ν. Therefore, the production term is altered as follows:

$$P = C_{b1}(1 - f_{t2})\bar{S}\bar{\nu} \tag{28}$$

where

$$f_{t2} = C_{t3}\exp\left(-C_{t4}\chi^2\right) \tag{29}$$

The other trip function is given by the source term $f_{t1}(\Delta q)^2$, which was derived from dimensional analysis, where

$$f_{t1} = C_{t1} g_t \exp\left\{-C_{t2}\left[\omega_t^2\big/(\Delta q)^2\right]\left(d^2 + g_t^2 d_t^2\right)\right\} \tag{30}$$

Here, Δq is the difference between velocities at the trip (zero at the wall) and the point in the field that is considered, ω_t is the vorticity at the wall at the trip point, d_t is the distance from the field point to the trip point, and g_t is given by

$$g_t = \min(0.1, \Delta q/\omega_t \Delta x) \tag{31}$$

where Δx is the grid spacing on the wall at the trip point. The closure coefficients are as follows:

$$\sigma = \tfrac{2}{3}, \qquad C_{b1} = 0.1355, \qquad C_{b2} = 0.622, \qquad C_{v1} = 7.1$$

$$C_{t1} = 1.0, \qquad C_{t2} = 2.0, \qquad C_{t3} = 1.1, \qquad C_{t4} = 2.0$$

$$C_{w1} = C_{b1}\big/\kappa^2 + (1 + C_{b2})/\sigma, \qquad C_{w2} = 0.3$$

$$C_{w3} = 2.0, \qquad \kappa = 0.41$$

V. Modification of the Turbulence Models for MHD Flows

A. Baldwin–Barth Turbulence Model

The derivation of the modified Baldwin–Barth turbulence model[30] is presented in this section. The Baldwin–Barth model was originally derived from the standard form of the $k - \epsilon$ model. Therefore, the modified version of the Baldwin–Barth model is derived from the existing modified $k - \epsilon$ model, for which the MHD effect is represented by additional magnetic terms in the turbulent equations.

Consider the incompressible $k - \epsilon$ model with magnetic terms. The k equation is

$$\frac{\mathrm{D}k}{\mathrm{D}t} = P_k - \epsilon + \frac{\partial}{\partial x_i}\left[\left(\nu + \frac{\nu_t}{\sigma_k}\right)\frac{\partial k}{\partial x_i}\right] + \frac{NM_k}{\rho} \tag{32}$$

The ϵ equation is

$$\frac{\mathrm{D}\epsilon}{\mathrm{D}t} = C_{\epsilon 1}\frac{\epsilon}{k}P_k - C_{\epsilon 2}\frac{\epsilon^2}{k} + \frac{\partial}{\partial x_i}\left[\left(\nu + \frac{\nu_t}{\sigma_\epsilon}\right)\frac{\partial\epsilon}{\partial x_i}\right] + \frac{NM_\epsilon}{\rho} \tag{33}$$

The effects of the magnetic field are modeled by the terms NM_k and NM_ϵ:

$$M_k = C'_{KN1} k B_i B_i \tag{34}$$

$$M_\epsilon = C'_{\epsilon N1}\epsilon B_i B_i \tag{35}$$

and N is the interaction parameter,

$$N = \sigma B^2 L/\rho U \tag{36}$$

In the Baldwin–Barth model, a new turbulent quantity is introduced, namely, the turbulent Reynolds number Re_T, which is defined as

$$Re_T = k^2/\nu\epsilon \tag{37}$$

Therefore,

$$\frac{\mathrm{d}(\nu Re_T)}{\nu Re_T} = 2\frac{\mathrm{d}k}{k} - \frac{\mathrm{d}\epsilon}{\epsilon} \tag{38}$$

This transformation can be applied for both the local derivative $\partial/\partial t$ and the convective derivative $\boldsymbol{U} \cdot \boldsymbol{\nabla}(\nu Re_T)$. Therefore, the substantial derivative satisfies the same transformation, that is,

$$\frac{1}{\nu Re_T}\frac{\mathrm{D}(\nu Re_T)}{\mathrm{D}t} = \frac{2}{k}\frac{\mathrm{D}k}{\mathrm{D}t} - \frac{1}{\epsilon}\frac{\mathrm{D}\epsilon}{\mathrm{D}t} \tag{39}$$

Substitution of Eqs. (32) and (33) into Eq. (39) yields

$$\frac{1}{\nu Re_T}\frac{\mathrm{D}(\nu Re_T)}{\mathrm{D}t} = \frac{2}{k}\left\{P_k - \epsilon + \frac{\partial}{\partial x_i}\left[\left(\nu + \frac{\nu_t}{\sigma_k}\right)\frac{\partial k}{\partial x_i}\right] + \frac{NM_k}{\rho}\right\}$$

$$-\frac{1}{\epsilon}\left\{C_{\epsilon 1}\frac{\epsilon}{k}P_k - C_{\epsilon 2}\frac{\epsilon^2}{k} + \frac{\partial}{\partial x_i}\left[\left(\nu + \frac{\nu_t}{\sigma_\epsilon}\right)\frac{\partial \epsilon}{\partial x_i}\right] + \frac{NM_\epsilon}{\rho}\right\} \tag{40}$$

Equation (40) can be rearranged by omitting some terms according to the discussion by Baldwin and Barth.[30] It can be shown that the two magnetic terms appearing in the $k-\epsilon$ model can be combined into one term for the Baldwin–Barth turbulence model. Therefore, only one closure coefficient needs to be adjusted. This new closure coefficient is defined as

$$C_{Re_T} = 2C'_{KN1} - C'_{\epsilon N1} \tag{41}$$

Thus, the effect of the magnetic field is modeled by the addition of the magnetic source term $(N/\rho)C_{Re_T}B_iB_i(\nu Re_T)$. The treatment of wall-bounded flows involves the introduction of damping terms in the production term and is assumed not to modify the magnetic term. Finally, the Baldwin–Barth turbulence model that accounts for the presence of a magnetic field is expressed as

$$\frac{\mathrm{D}(\nu Re_T)}{\mathrm{D}t} = (C_{\epsilon 1} - C_{\epsilon 2})\sqrt{\nu Re_T P_k} + \left(\nu + \frac{\nu_t}{\sigma_k}\right)\nabla^2(\nu Re_T)$$

$$-\frac{1}{\sigma_\epsilon}(\nabla\nu_t)[\nabla(\nu Re_T)] + \frac{N}{\rho}C_{Re_T}B^2(\nu Re_T) \tag{42}$$

The closure coefficient associated with the additional magnetic term has been calibrated for the MHD Hartmann flow (Sec. VI.A), and its proposed value is $C_{Re_T} = 6.0$.

B. Spalart–Allmaras Turbulence Model

The approach to modify the Spalart–Allmaras turbulence model[31] in the presence of a magnetic field is different from the proposed modification concerning the Baldwin–Barth turbulence model. Here, no additional magnetic term is added to the partial differential equation governing the variable $\bar{\nu}$. Rather, the effect of the magnetic field is accounted for within the closure coefficient C_{v1}, which becomes a function of the magnetic field. The motivation behind this approach lies in that the Spalart–Allmaras model is the model that performs the best in the prediction of the relaminarization process of the MHD Hartmann flow. In fact, when the model is used in its original form, it only slightly overpredicts the relaminarization process. Therefore, instead of designing an additional magnetic term, it is proposed that an adjustment in the closure coefficient would be sufficient to extend the Spalart–Allmaras model to MHD flows.

As for the Baldwin–Barth turbulence model, the objective of the proposed modification is to reduce the amount of turbulent viscosity. This can be accomplished by several mechanisms. The Spalart–Allmaras model solves an equation in terms of the turbulent quantity $\bar{\nu}$, which is directly related to the turbulent viscosity through the function f_{v1}. Therefore, it would be suitable to make f_{v1} a decreasing function of the magnetic strength. Another option would be to decrease the production of $\bar{\nu}$, or increase the dissipation of $\bar{\nu}$, or a combination of both. Based on the analysis of the Hartmann flow (Sec. VI.B), it is proposed to modify the closure coefficient C_{v1} according to the following equation:

$$C_{v1} = 7.1\min\{2.6 + 1.6\tanh[4{,}430(Ha/Re) - 19.345]$$

$$+ 22.0(Ha/Re);\ 4{,}225\} \tag{43}$$

VI. Results

A. MHD Hartmann Flow

The Hartmann flow is utilized to calibrate the turbulence models. The Hartmann flow refers to the fully developed flow between two parallel plates subject to a magnetic field. A pressure gradient drives the fluid into motion and balances the viscous and magnetic friction. Consider an incompressible fluid, with constant viscosity and constant electrical conductivity flowing between two infinite parallel flat plates (Fig. 1). A constant magnetic field is applied in the transverse direction, that is, the y direction. All variables are functions of y only, except the pressure. The walls are located at $y = \pm h$. Laminar and turbulent flows are investigated. The flow conditions are summarized in Table 1.

The Reynolds number based on the half-height h between the two plates and the average velocity, ranges from 5×10^3–5×10^4. The magnetic Reynolds number corresponding to these conditions is $Re_m = 1.51 \times 10^{-4}$. Therefore, the induced magnetic field can be considered negligible compared to the applied magnetic field. The loading factor is zero, that is, there is no applied electric field.

The computation is performed on a two-dimensional domain. The ratio between the length and the height of the domain is $L/2h = 10$, and the number of grid points is 10 in the x direction with uniform grid spacing. The grid has been generated analytically.

There are 150 grid points in the y direction, and grid clustering is implemented near the two solid walls to resolve the velocity gradients. The velocity is extrapolated at the inlet and outlet to obtain a fully developed flow in a short computational time. The boundary conditions at the wall are specified as no-slip condition for the velocity, and the wall is adiabatic. The pressure gradient in the x direction is adjusted to provide the same mass flow rate regardless of the strength of the magnetic field.

Figure 2 shows the fully developed velocity profiles for different values of the Hartmann number in the laminar case, for which a comparison with the analytical solution is possible. The velocities are normalized with the maximum velocity obtained in the nonmagnetic laminar case. When $Ha = 0.0$, the well-known parabolic profile corresponding to the couette flow in fluid dynamics is obtained. As the Hartmann number is increased, the velocity profiles are flattened, and the maximum velocity (at the centerline) is decreased. For Hartmann numbers greater than 10.0, the velocity remains almost constant on a large region between the two flat plates. It can be qualitatively observed by inspecting the velocity slopes at the walls that the skin friction increases with the Hartmann number. In all cases, the computed solutions are in excellent agreement with the analytical results.[32]

Table 1 Properties of the MHD Hartmann flow

Property	Value
Density ρ	1.225 kg/m^3
Electrical conductivity σ_e	800 mho/m
Viscosity μ	1.8×10^{-5} kg/(m · s)
Distance between the plates h	0.005 m

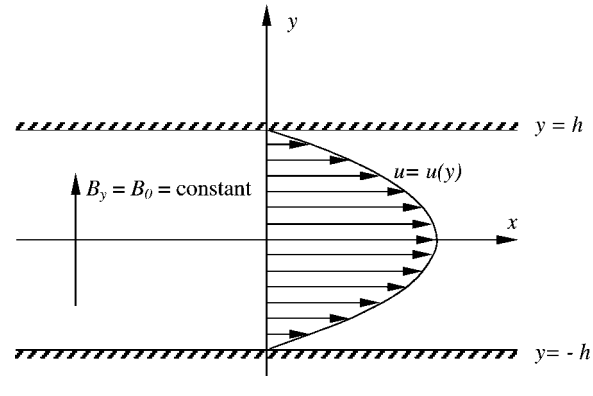

Fig. 1 Schematic of the Hartmann flow.

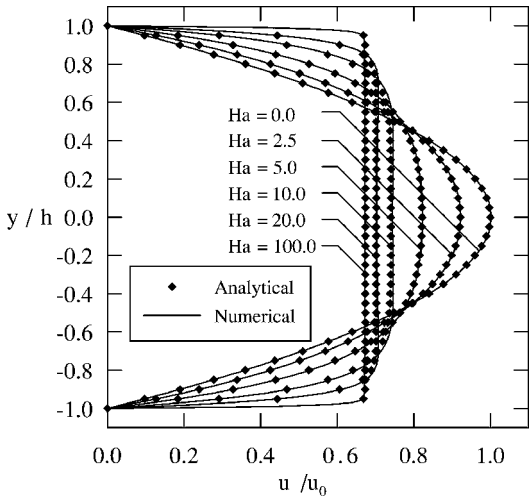

Fig. 2 Laminar velocity profiles for the Hartmann flow.

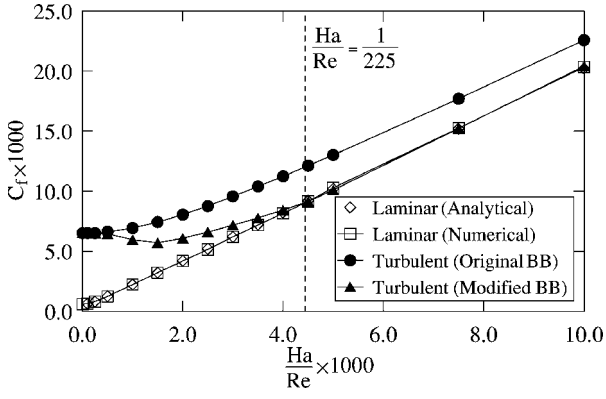

Fig. 3 Skin-friction coefficient for the Hartmann flow at $Re = 1.0 \times 10^4$.

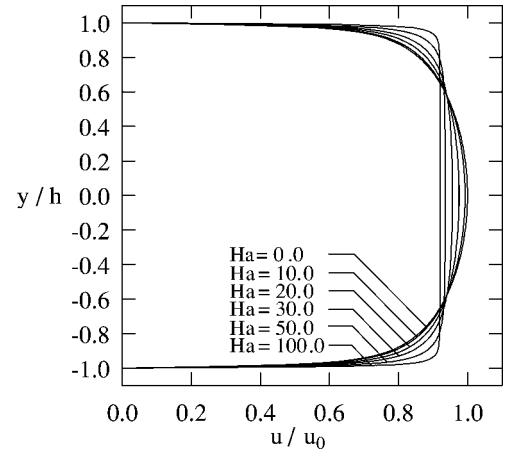

a) Original Baldwin–Barth model

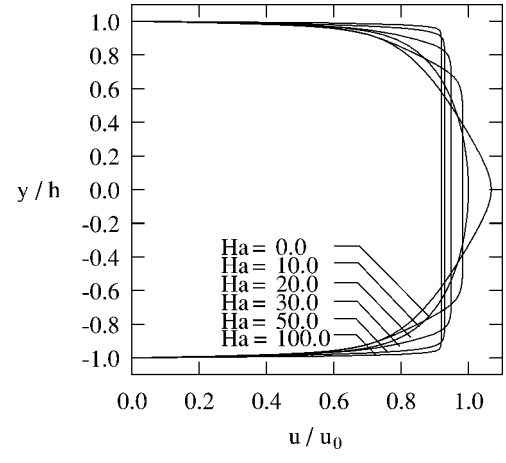

b) Modified Baldwin–Barth model

Fig. 4 Turbulent velocity profiles.

In the case of a turbulent flow, it has been experimentally shown by Brouillette and Lykoudis[33] that a relaminarization process should occur when the magnetic field is sufficiently strong. The criterion for the relaminarization process is expressed by the ratio of the Hartmann number to the Reynolds number. The advantage of expressing the relaminarization criterion with this ratio is that it becomes independent of the reference length. Brouillette and Lykoudis found that when the critical value of $Ha/Re = 1/225$ is reached, the flow should return to a laminar state. One of the objectives of this investigation is to reproduce this experimental conclusion. Although the results obtained by Brouillette and Lykoudis were for liquid metal flows, they are utilized as a first attempt to calibrate the computer code. Additional experimental data will be required to calibrate the numerical code for a wider range of applications.

1. *Baldwin–Barth Turbulence Model*

Figure 3 shows the skin-friction coefficient vs Ha/Re for a Reynolds number of 1×10^4. In the case of the laminar flow, the computed values compare well with the analytical solution. Note that, for large values of the Hartmann number, the skin-friction coefficient can be approximated by the straight line $2Ha/Re$. In the case of the turbulent flow, the skin friction obtained with the original Baldwin–Barth model[30] does not show any relaminarization process, the turbulent skin friction always remains greater than the laminar one. When the magnetic terms are included in the turbulent equations, the modified version predicts that a relaminarization process occurs at $Ha/Re = 1/225$, matching the experimental results of Brouillette and Lykoudis.[33] The closure constant C_{Re_T} appearing in the magnetic terms of the modified model has been calibrated to provide this result ($C_{Re_T} = 6.0$). Figure 4 shows the velocity profiles for the original and modified models. For moderate Hartmann number, there is an increase in the maximum velocity when the modified model is used, whereas the original model always provided a flattening of the profiles as the Hartmann number is increased. The turbulent viscosity decreases as the Hartmann number is increased when the original model is used (Fig. 5a), and some turbulent viscosity is still present in the flow at high Hartmann numbers, which does not enable the flow to become laminar again. The modified version decreases the turbulent viscosity more substantially, especially in the center region of the flow (Fig. 5b). Note that at $Ha/Re = 1/225$ the maximum turbulent viscosity is decreased to the point that it becomes negligible in the case of the modified model (Fig. 6), whereas the flow remains turbulent even at very large Hartmann numbers for the original model.

The Baldwin–Barth model behaves similarly for Reynolds numbers ranging from 5×10^3 to 5×10^4 (Fig. 7). The original model is not able to predict the relaminarization, whereas the modified version does.

2. *Spalart–Allmaras Turbulence Model*

The skin friction obtained with the Spalart–Allmaras model[31] at $Re = 1 \times 10^4$ is shown in Fig. 8. With the original model, the turbulent skin friction almost recovers the laminar skin friction values when $Ha/Re \approx 6 \times 10^{-3}$, which is larger than the experimental prediction of Brouillette and Lykoudis,[33] as shown by the vertical dashed line. However, it always remains slightly greater than its laminar counterpart. To match the experimental result illustrating the relaminarization process, a modification of the Spalart–Allmaras closure coefficient C_{v1} is proposed. This closure coefficient influences the production term in the turbulence model and the evaluation of the turbulent viscosity from the turbulent quantity $\bar{\nu}$. An increase of this coefficient decreases the production of turbulent viscosity. When the closure coefficient C_{v1} is made dependent on the Hartmann number, it is possible to reproduce the relaminarization

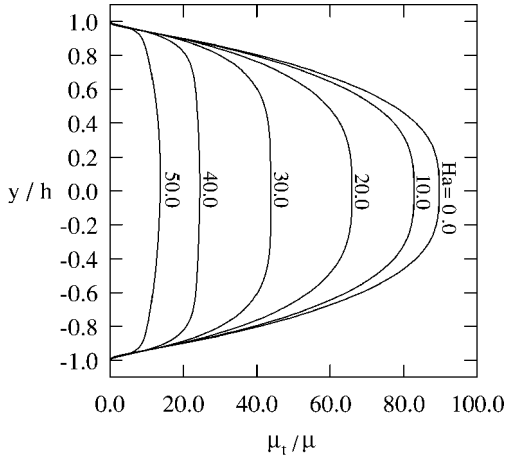

a) Original Baldwin–Barth model

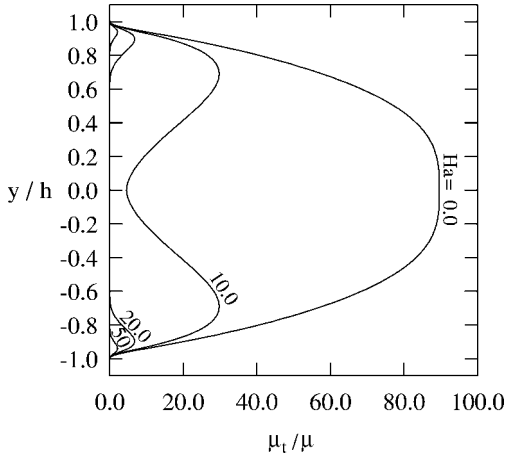

b) Modified Baldwin–Barth model

Fig. 5 Turbulent viscosity profiles.

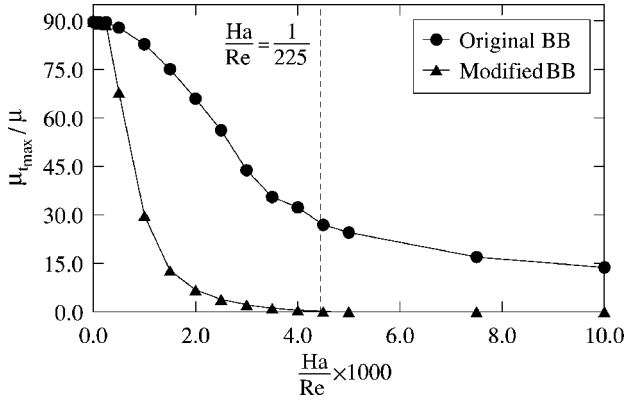

Fig. 6 Maximum turbulent viscosity.

criterion of $Ha/Re = 1/225$. Figure 9 shows the dependence of the closure coefficient C_{v1} on the Hartmann number. The proposed relation between C_{v1} and Ha/Re is provided by Eq. (43). A substantial increase in the coefficient C_{v1} is required in the relaminarization region to obtain the anticipated effect.

The effect of this modification on the production, dissipation, and diffusion terms in the Spalart–Allmaras turbulence model is shown in Fig. 10. All quantities have been normalized with their nonmagnetic counterparts. As the coefficient C_{v1} increases, the production and diffusion terms are reduced, up to a little less than 10%. On the other hand, the dissipation term increases by about 10%, leading to a reduction in the turbulent quantity $\bar{\nu}$ by about 20%.

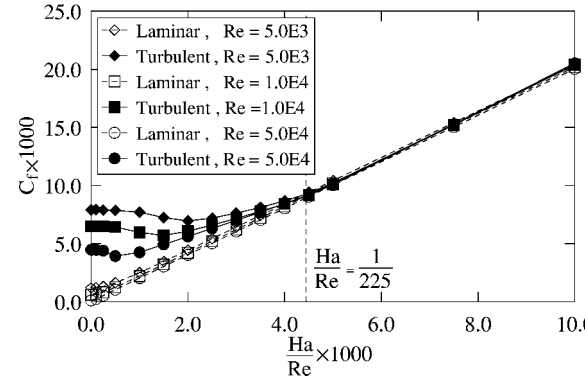

Fig. 7 Summary of skin-friction coefficient for the Hartmann flow.

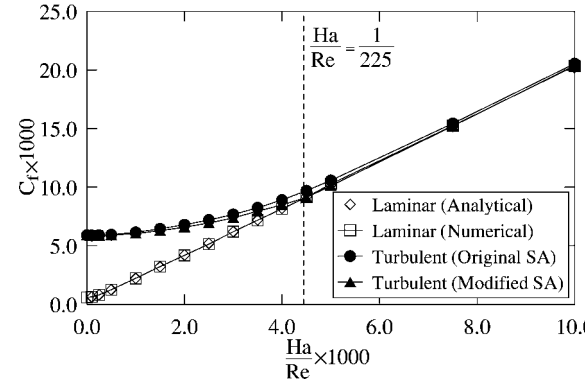

Fig. 8 Skin-friction coefficient for the Hartmann flow at $Re = 1.0 \times 10^4$ (Spalart–Allmaras model).

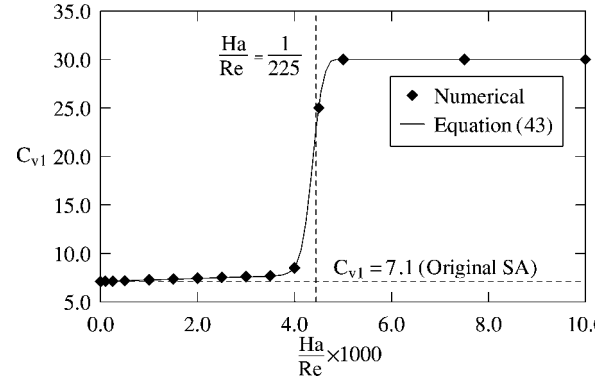

Fig. 9 Closure coefficient C_{v1} for the modified Spalart–Allmaras model.

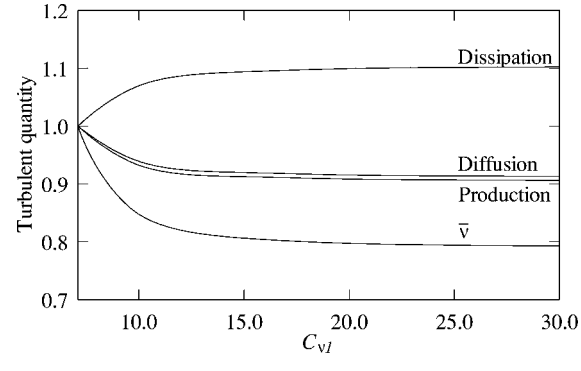

Fig. 10 Effect of the closure coefficient C_{v1} on the turbulent terms of the Spalart–Allmaras model.

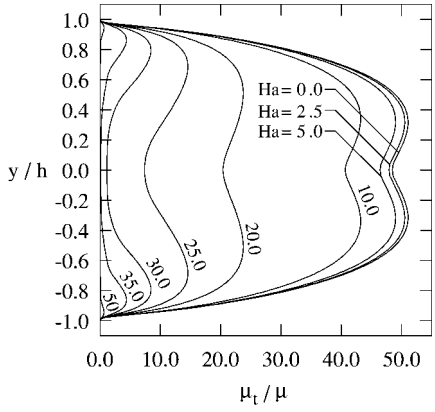

a) Original Spalart–Allmaras model

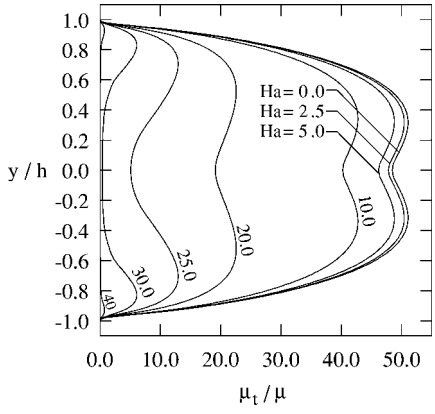

b) Modified Spalart–Allmaras model

Fig. 11 Turbulent viscosity profiles.

The turbulent viscosity profiles are shown in Fig. 11 for the original and modified models, respectively. The general shape of the profile shows that the turbulent viscosity first increases away from the wall and then exhibits a local minimum at the centerline. As Hartmann number Ha is increased, the amount of turbulent viscosity is naturally decreased until it is sufficiently small to initiate the relaminarization process. For the original Spalart–Allmaras model, the turbulent viscosity becomes negligible when Ha reaches a value of 50.0. The turbulent viscosity profiles obtained by the modified Spalart–Allmaras model are very similar to those obtained by the original model. The difference between the two models becomes noticeable for Ha greater than 20.0, where the amount of turbulent viscosity is further reduced by the higher values of C_{v1} in the modified model. The turbulent viscosity becomes negligible when Ha reaches a value of 40, when the relaminarization process is about to occur.

Another illustration of the differences between the original and modified Spalart–Allmaras models is shown in Fig. 12, where the maximum values of the turbulent viscosity are plotted vs Ha/Re. For small values of Ha/Re, no noticeable change is observed, and both models provide identical turbulent viscosities. It is followed by a rapid decrease in the maximum turbulent viscosity when the magnetic field is increased. At the relaminarization point, the modified Spalart–Allmaras model provides a sufficiently small turbulent viscosity, whereas the original model is not adapted to meet the relaminarization criterion exactly, providing too large a turbulent viscosity, the relaminarization process being reached for larger values of the Hartmann number.

B. Supersonic Flow over a Flat Plate

The objective of this section is to investigate the effect of the magnetic field on the skin friction for a supersonic turbulent flow over a flat plate. The freestream conditions are summarized in Table 2. The length of the flat plate is 0.08 m, and the transition is triggered

Table 2 Freestream conditions over the flat plate

Property	Value
Mach number M_∞	2.0
Pressure p_∞	1.0 atm
Temperature T_∞	300.0 K
Reynolds number Re_∞	3.75×10^6
Electrical conductivity $\sigma_{e\infty}$	800 mho/m

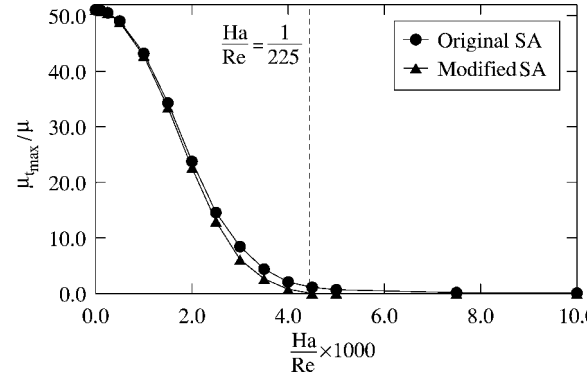

Fig. 12 Maximum turbulent viscosity (Spalart–Allmaras model).

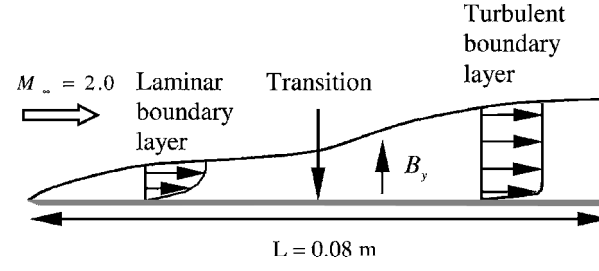

Fig. 13 Schematic of the flow over a flat plate.

at $x = 0.04$ m, The magnetic Reynolds number based on the length of the flat plate is $Re_m = 0.058$, which can be considered negligible. Therefore, the MHD equations will be solved by the low magnetic Reynolds number formulation. A schematic of a typical flow is shown in Fig. 13. Note that the specified value of the electrical conductivity will be too large from a practical point of view, but was selected in the present investigation due to stability requirement. In practice, the same interaction number could be achieved by simultaneously decreasing the electrical conductivity and increasing the magnetic field intensity.

The grid system consists of 100 grid points in the x direction and 50 grid points in the y direction. Grid point clustering has been implemented near the leading edge to capture the weak leading-edge shock wave and near the solid surface to resolve the laminar and turbulent boundary layers. The first value of y^+ away from the wall is about one over the length of the flat plate. The grid system, which was generated analytically, is shown in Fig. 14. In terms of boundary conditions, a zero velocity is specified at the wall. The pressure and temperature are extrapolated at the wall, that is, the pressure gradient normal to the wall is set to zero, and the plate is considered to be adiabatic.

The magnetic field is applied in the y direction, ranging from 0 to 1.4 T. The strength of the magnetic field can be represented either by the magnitude of the applied magnetic field B_y, or by the interaction parameter defined as

$$m = \sigma_{e\infty} B_y^2 \big/ \rho_\infty U_\infty \tag{44}$$

The turbulence models are initially investigated for the nonmagnetic case. Figure 15 shows the skin-friction coefficient along the flat plate. Because the transition from laminar to turbulent flow is triggered at $x = 0.04$ m, the laminar skin friction, from the leading

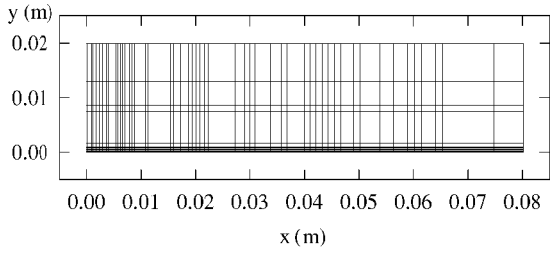

Fig. 14 Grid system (100 × 50 grid points).

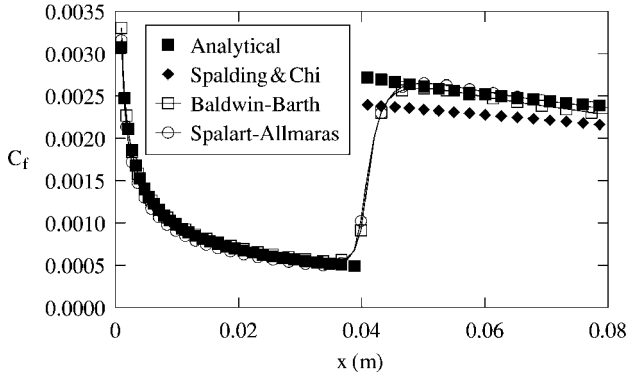

Fig. 15 Comparison of the turbulence models in the nonmagnetic case.

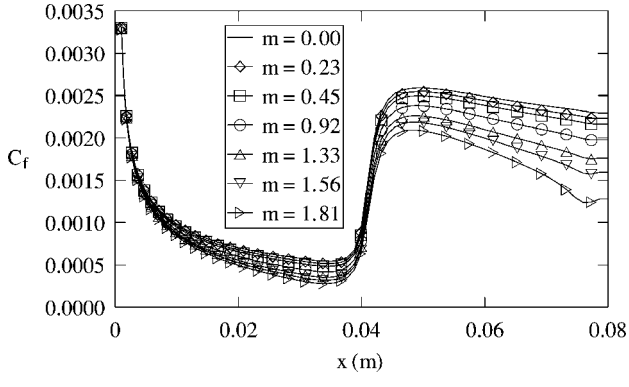

a) Original Baldwin–Barth model

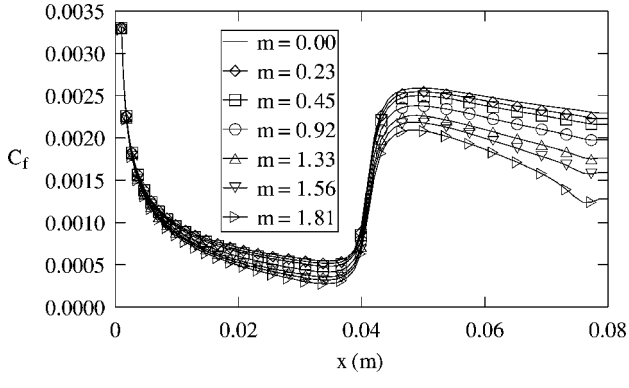

b) Modified Baldwin–Barth model

Fig. 16 Skin-friction coefficients.

edge to the transition point, does not depend on the turbulence model. In the turbulent region, both turbulence models provide a skin-friction coefficient that is between the analytical solution and the semi-empirical method of Spalding and Chi.[34]

Next, the magnetic field is applied uniformly in the y direction. Figure 16a shows the skin-friction coefficient obtained by the original Baldwin–Barth model[30] for several values of the magnetic field. The skin friction is decreased in the laminar region as the magnetic field is increased. The same effect can be observed in the turbulent region. However, no relaminarization process is achieved because the skin friction does not reach a sufficiently low value. The modified Baldwin–Barth model[31] provides similar skin-friction distributions (Fig. 16b). The turbulent skin friction is slightly lower than those obtained by the original model. To understand why the full relaminarization process does not occur, the velocity profiles are examined. First, the laminar velocity profiles are plotted at $x = 0.06$ m (Fig. 17a). These profiles were obtained by considering a fully laminar flow along the flat plate. The effect of the magnetic field is to generate a Lorentz force acting in the opposite direction of the incoming flow. Therefore, the flow is decelerated as the magnetic field is increased. For a sufficiently large value of the magnetic field, it leads to a separation of the flow, at $m = 1.33$. The freestream velocity is also reduced as the magnetic field increases because the magnetic field remains constant within the entire domain. Once the flow is separated, it is not possible to obtain a converged solution because a large subsonic region develops, which reaches the boundaries of the computational domain. The boundary conditions, based on a supersonic inflow and outflow, are not suitable for such a flow.

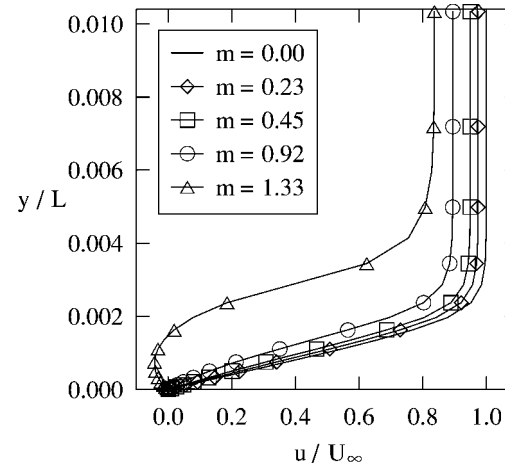

a) Laminar

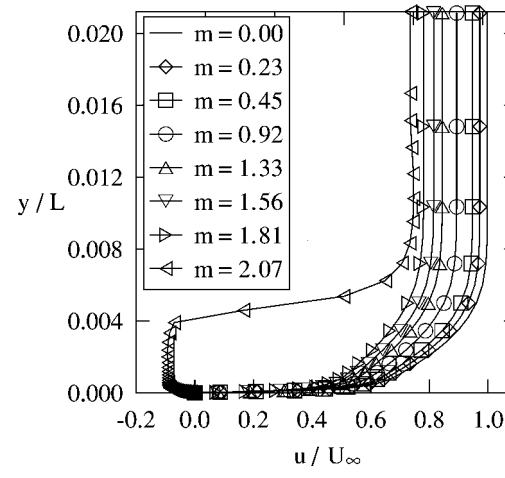

b) Turbulent

Fig. 17 Velocity profiles at x = 0.06 m.

Figure 17b shows the turbulent velocity profile obtained by the original Baldwin–Barth turbulence model, at $x = 0.06$ m. In the turbulent case, it is possible to increase the magnetic field up to $m = 1.81$, after which a massive separation occurs. The separation occurs for larger values of the applied magnetic field than for the laminar case because the turbulent layer can sustain a stronger Lorentz force. This is similar to the comparison between laminar and turbulent boundary layers subject to an adverse pressure gradient. The separation is delayed when the boundary layer is turbulent.

Similar results are obtained with the Spalart–Allmaras turbulence models. Figure 18a illustrates how the skin-friction coefficient

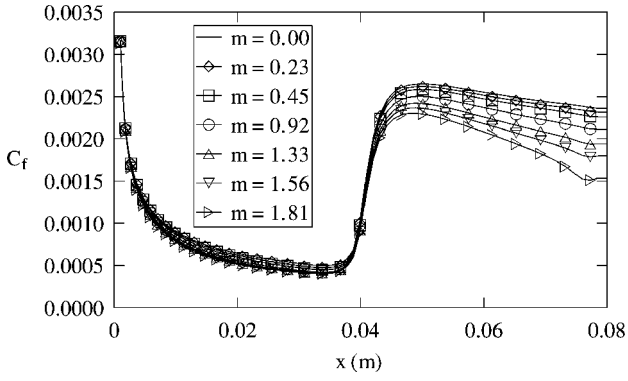

a) Original Spalart–Allmaras

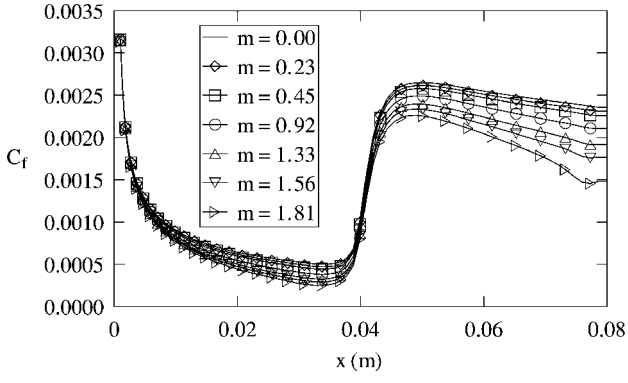

b) Modified Spalart–Allmaras

Fig. 18 Skin-friction coefficients.

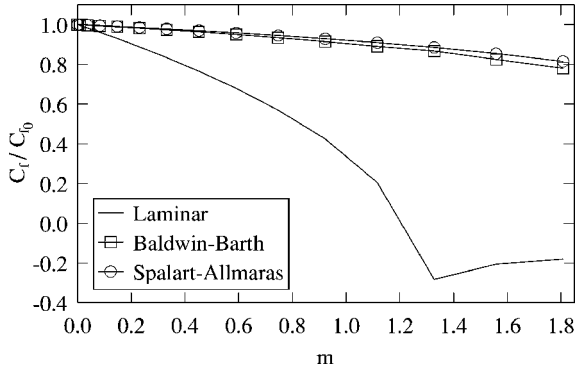

Fig. 19 Skin-friction coefficient ratios obtained by the original turbulence models.

decreases as the magnetic field is increased. The modified version provides a slightly lower skin friction than the original version, but no relaminarization process occurs. Figure 19 shows the relative skin friction at a given location ($x = 0.06$ m), when it is normalized with its nonmagnetic counterpart. In the laminar case, the relative reduction of the skin friction is more important than in the turbulent case. A substantial reduction is achieved, which leads to the separation of the flow (negative value of the skin friction). In the turbulent case, a reduction of up to about 20% is achieved with all turbulence models, at the highest value of magnetic field. Similar results are obtained with the modified versions of the turbulence models (not shown). A complete relaminarization of the flow cannot be achieved because the effects of the magnetic field on the mean flow are larger than the effects on the small scales of motion. The present effort focused on the implementation of the turbulence models for MHD flows and the possibility to calibrate a given turbulence model for a specific application. Although a reduction in the skin friction is achieved, nonideal effects such as Hall effect and ion slip may limit the gain obtained by application of the magnetic field.

VII. Conclusions

The computation of the turbulent Hartmann flow using the Baldwin–Barth and Spalart–Allmaras one-equation turbulence models was presented. The low magnetic Reynolds number formulation was implemented for low electrical conductivity fluids. Because the original Baldwin–Barth turbulence model is not designed for MHD flows, it is not able to predict the relaminarization process accurately. A modified version was proposed to account for the presence of a magnetic field. It was directly derived from an existing modified $k - \epsilon$ model. One additional magnetic term, along with its corresponding closure coefficient, represents the effect of the magnetic field. After calibration, the modified version was able to decrease sufficiently the level of turbulent viscosity and accurately predict the relaminarization process. The original Spalart–Allmaras model only slightly overpredicted the skin friction. Therefore, a simpler approach was considered to account for the presence of the magnetic field, where one closure coefficient was made dependent on the magnetic field. This simple modification proved to be sufficient to predict accurately the relaminarization process in the case of the Hartmann flow. Little difference was observed between the original and modified versions of the turbulence models for the supersonic flow over a flat plate. Although a reduction in the skin-friction coefficient of up to 20% can be achieved by the application of a magnetic field, no relaminarization process occurred.

Acknowledgments

This work was sponsored by the U.S. Air Force Office of Scientific Research under tasks monitored by John Schmisseur. The authors acknowledge the support of Kansas National Science Foundation Cooperative Agreement EPS-9874732 and the Wichita State University High Performance Computing Center.

References

[1]Rossow, V. J., "On Flow of Electrically Conducting Fluids Over a Flat Plate in the Presence of a Transverse Magnetic Field," NACA TN 3971, May 1957.

[2]Lykoudis, P. S., "On a Class of Compressible Laminar Boundary Layers with Pressure Gradient for an Electrically Conducting Fluid in the Presence of a Magnetic Field," *Proceedings of the 9th Annual Congress of the International Astronautical Federation*, Springer-Verlag, Vienna, 1959, pp. 168–180.

[3]Bleviss, Z. O., "Magnetogasdynamics of Hypersonic Couette Flow," *Journal of the Aero/Space Sciences*, Vol. 25, No. 10, 1958, pp. 601–615.

[4]Bush, W. B., "Magnetohydrodynamic-Hypersonic Flow past a Blunt Body," *Journal of the Aero/Space Sciences*, Vol. 25, No. 11, 1958, pp. 685–690.

[5]Lykoudis, P. S., "The Newtonian Approximation in Magnetic Hypersonic Stagnation-Point Flow," *Journal of the Aero/Space Science*, Vol. 28, No. 7, 1961, pp. 541–546.

[6]Palmer, G., "Magnetic Field Effects on the Computed Flow over a Mars Return Aerobrake," *Journal of Thermophysics and Heat Transfer*, Vol. 7, No. 2, 1993, pp. 294–301.

[7]Zachary, A. L., and Collella, P., "A Higher-Order Godunov Method for the Equations of Ideal Magnetohydrodynamics," *Journal of Computational Physics*, Vol. 99, No. 2, 1992, pp. 341–347.

[8]Bell, J. B., Colella, P., and Trangenstein, J. A., "High Order Godunov Methods for General Systems of Hyperbolic Conservation Laws," *Journal of Computational Physics*, Vol. 82, No. 2, 1989, pp. 362–397.

[9]Brio, M., and Wu, C. C., "An Upwind Differencing Scheme for the Equations of Ideal Magnetohydrodynamics," *Journal of Computational Physics*, Vol. 75, No. 2, 1998, pp. 400–422.

[10]Dai, W., and Woodward, P. R., "Extension of the Piecewise Parabolic Method to Multidimensional Ideal Magnetohydrodynamics," *Journal of Computational Physics*, Vol. 115, No. 2, 1994, pp. 485–514.

[11]Dai, W., and Woodward, P. R., "A Simple Riemann Solver and High-Order Godunov Schemes for Hyperbolic Systems of Conservation Laws," *Journal of Computational Physics*, Vol. 121, No. 1, 1995, pp. 51–65.

[12]Dai, W., and Woodward, P. R., "A Second-Order Iterative Implicit-Explicit Hybrid Scheme for Hyperbolic Systems of Conservation Laws," *Journal of Computational Physics*, Vol. 128, No. 1, 1996, pp. 181–196.

[13]Harada, S., Augustinus, J., Hoffmann, K. A., and Agarwal, R. K., "Development of a Modified Runge-Kutta Scheme with TVD Limiters for the Ideal 1-D MHD Equations," AIAA Paper 97-2090, June 1997.

[14]Augustinus, J., Harada, S., Hoffmann, K. A., and Agarwal, R. K., "Numerical Solution of the Eight-Wave Structure Ideal MHD Equations by Modified Runge–Kutta Scheme with TVD," AIAA Paper 97-2398, June 1997.

[15]Augustinus, J., Hoffmann, K. A., and Harada, S., "Effect of Magnetic Field on the Structure of High-Speed Flows," *Journal of Spacecraft and Rockets*, Vol. 35, No. 5, 1998, pp. 639–646.

[16]Harada, S., Hoffmann, K. A., and Augustinus, J., "Numerical Solution of the Ideal Magnetohydrodynamics Equations for a Supersonic Channel Flow," *Journal of Thermophysics and Heat Transfer*, Vol. 12, No. 4, 1998, pp. 507–513.

[17]Harada, S., Hoffmann, K. A., and Augustinus, J., "Development of a Modified Runge–Kutta Scheme with TVD Limiters for the Ideal Two-Dimensional MHD Equations," AIAA Paper 98-0981, Jan. 1998.

[18]Powell, K. G., Roe, P. L., Myong, R. S., Gombosi, T., and De Zeeuw, D., "An Upwind Scheme for Magnetohydrodynamics," AIAA Paper 95-1704, June 1995.

[19]Hoffmann, K. A., Damevin, H. M., and Dietiker, J. F., "Numerical Simulation of Hypersonic Magnetohydrodynamic Flows," AIAA Paper 2000-2259, June 2000.

[20]Ferraro, V. C. A., and Plumton, C., *Magneto-Fluid Mechanics*, Oxford Univ. Press, Oxford, 1966.

[21]Lykoudis, P. S., "Transition from Laminar to Turbulent Flow in Magneto-Fluid Mechanic Channels," *Review of Modern Physics*, Vol. 32, No. 4, 1960, pp. 796–798.

[22]Lykoudis, P. S., "Magneto Fluid Mechanics Channel Flow. II. Theory," *Physics of Fluids*, Vol. 10, No. 5, 1967, pp. 1002–1007.

[23]Lee, M. L., Lee, S. J., and Kim, C. T., "Numerical and Experimental Investigation of Flow Channel," *Progress in Fluid Flow Research: Turbulence and Applied MHD*, Vol. 182, Progress in Astronautics and Aeronautics, AIAA Reston, VA, 1998, pp. 437–453.

[24]Frando, S., "Study of the MHD Turbulent Flow in Electromagnetic Valve," *Progress in Fluid Flow Research: Turbulence and Applied MHD*, Vol. 182, Progress in Astronautics and Aeronautics, AIAA Reston, VA, 1998, pp. 563–576.

[25]El-Kaddah, N., "The Turbulent Recirculating Flow Field in a Coreless Induction Furnace, A Comparison of Theoretical Predictions with Measurements," *Journal of Fluid Mechanics*, Vol. 133, No. 37, 1983, pp. 37–46.

[26]Gaitonde, D. V., and Poggie, J., "An Implicit Technique for 3-D Turbulent MGD with the Generalized Ohm's Law," AIAA Paper 2001-2736, June 2001.

[27]Shimomura, Y., "Statistical Analysis of Magnetohydrodynamic Turbulent Shear Flows at Low Magnetic Reynolds Number," *Journal of the Physical Society of Japan*, Vol. 57, No. 7, 1988, pp. 2365–2385.

[28]Lesieur, M., and Comte, P., "Large Eddy Simulations of Compressible Turbulent Flows," *Turbulence in Compressible Flows*, AGARD Rept. 819, 1997, Chap. 4.

[29]Hoffmann, K. A., and Chiang, S. T., *Computational Fluid Dynamics*, 4th ed., Vol. 2, Engineering Education System, Wichita, KS, 2001.

[30]Baldwin, B. S., and Barth, T. J., "A One-Equation Turbulent Transport Model for High Reynolds Number Wall-Bounded Flows," NASA TM 102847, Aug. 1990.

[31]Spalart, P. R., and Allmaras, S. R., "A One-Equation Turbulence Model for Aerodynamic Flows," AIAA Paper 92-0439, Jan. 1992.

[32]Moreau, R., *Magnetohydrodynamics*, Kluwer Academic, Dordrecht, The Netherlands, 1990.

[33]Brouillette, E. C., and Lykoudis, P. S., "Magneto Fluid Mechanics Channel Flow. I Experiment," *Physics of Fluids*, Vol. 10, No. 5, 1967, pp. 995–1001.

[34]Spalding, D. B., and Chi, S. W, "The Drag of a Compressible Turbulent Boundary Layer on a Smooth Plate with and without Heat Transfer," *Journal of Fluid Mechanics*, Vol. 18, No. 1, 1964, pp. 117–143.